nature structural & molecular biology

Structural basis for interaction of a cotranslational chaperone with the eukaryotic ribosome

Yixiao Zhang[1], Chengying Ma[1], Yi Yuan[1], Jing Zhu[2], Ningning Li[1], Chu Chen[1], Shan Wu[1], Li Yu[2], Jianlin Lei[1] & Ning Gao[1]

Cotranslational chaperones, ubiquitous in all living organisms, protect nascent polypeptides from aggregation and facilitate their *de novo* folding. Importantly, emerging data have also suggested that ribosome-associated cotranslational chaperones have active regulatory roles in modulating protein translation. By characterizing the structure of a type of eukaryotic cotranslational chaperone, the ribosome-associated complex (RAC) from *Saccharomyces cerevisiae*, we show that RAC cross-links two ribosomal subunits, through a single long α-helix, to limit the predominant intersubunit rotation required for peptide elongation. We further demonstrate that any changes in the continuity, length or rigidity of this middle α-helix impair RAC function *in vivo*. Our results suggest a new mechanism in which RAC directly regulates protein translation by mechanically coupling cotranslational folding with the peptide-elongation cycle, and they lay the foundation for further exploration of regulatory roles of RAC in translation control.

After nascent polypeptides emerge from the ribosome, growing chains are in an aggregation-prone and partially folded state. Productive folding requires ribosome-associated chaperones to prevent non-native interactions[1,2]. There are two systems of cotranslational chaperones in eukaryotic cells: RAC and the nascent chain–associated complex (NAC)[2,3]. RAC is universally present in eukaryotes from yeast to humans[4,5]. The yeast RAC is composed of HSP40 (Zuotin) and HSP70 (Ssz), which coordinate with another HSP70 member (Ssb1 or Ssb2, collectively referred to as Ssb hereafter), as a functional triad (Ssz–Zuotin–Ssb) to facilitate early folding of nascent peptides[6]. The conserved function of RAC–Ssb requires the integrity of all three components because deletion of any single one induces generally similar cellular disorders related to protein-folding stress, for example, sensitivity to cold and salt[6–10]. Ssz is a specialized HSP70 that lacks ATPase activity at the N-terminal domain (NTD), and its putative substrate-binding C-terminal domain (CTD) is dispensable for its function[10,11]. The direct role of Ssb in cotranslational folding requires the cochaperone RAC as a whole[11], and the J domain of Zuotin in particular is essential for the ATPase stimulation of Ssb[12].

Although the primary function of Ssz–Zuotin–Ssb is known, molecular details, as well as their potential interplay with other nascent peptide–processing systems[2,13], remain to be explored. More importantly, accumulating data have also shown that RAC–Ssb is directly involved in translation modulation and nascent-peptide quality control under various growth conditions[3,13–18], but the underlying mechanisms are largely unknown. Notably, RAC has also been implicated in other highly regulated pathways related to growth control, such as ribosome biogenesis[19,20] and quorum sensing[21,22]. Therefore, the structural characterization of RAC on the ribosome is crucial for further dissection and understanding of these diverse functions of RAC. A previous cryo-EM structure of the *Chaetomium thermophilum* 80S ribosome bound with RAC is available[23]; however, the relatively low occupancy of RAC has prevented full depiction of the RAC-80S interaction and elucidation of the underlying functional implications. Most of the functional studies of RAC have been carried out in the yeast system. We therefore sought to determine the structure of RAC in complex with the 80S ribosome from *S. cerevisiae*.

RESULTS

Overview of the cryo-EM structure of the 80S–RAC complex

We reconstituted ribosomal complexes of 80S–RAC and 80S–Zuotin from purified components and subjected them to cryo-EM single-particle analysis. To improve the occupancy of RAC or Zuotin on the 80S ribosome, we tested different batches of purified components (**Supplementary Table 1**). As a result, we obtained structures of the empty 80S, 80S–Zuotin and 80S–RAC complexes (**Supplementary Fig. 1**). Comparison of these structures immediately identified densities from RAC or Zuotin alone. Consistently with the solution small-angle X-ray scattering data[23], RAC displays a highly extended conformation spanning nearly 190 Å on the ribosome. Interestingly, both the NTD and CTD of Zuotin interact with the ribosome. The two distal domains of Zuotin are connected by a rod-like mass, which bridges the two subunits. In contrast, Ssz is free of ribosomal contact and is anchored to the ribosome through direct interaction with the Zuotin NTD (**Supplementary Fig. 1** and **Supplementary Movie 1**).

[1]Ministry of Education Key Laboratory of Protein Sciences, Center for Structural Biology, School of Life Sciences, Tsinghua University, Beijing, China. [2]State Key Laboratory of Biomembrane and Membrane Biotechnology, Tsinghua University–Peking University Center for Life Sciences, Tsinghua University, Beijing, China. Correspondence should be addressed to N.G. (ninggao@tsinghua.edu.cn) or J.L. (jllei@tsinghua.edu.cn).

Received 17 June; accepted 30 September; published online 2 November 2014; doi:10.1038/nsmb.2908

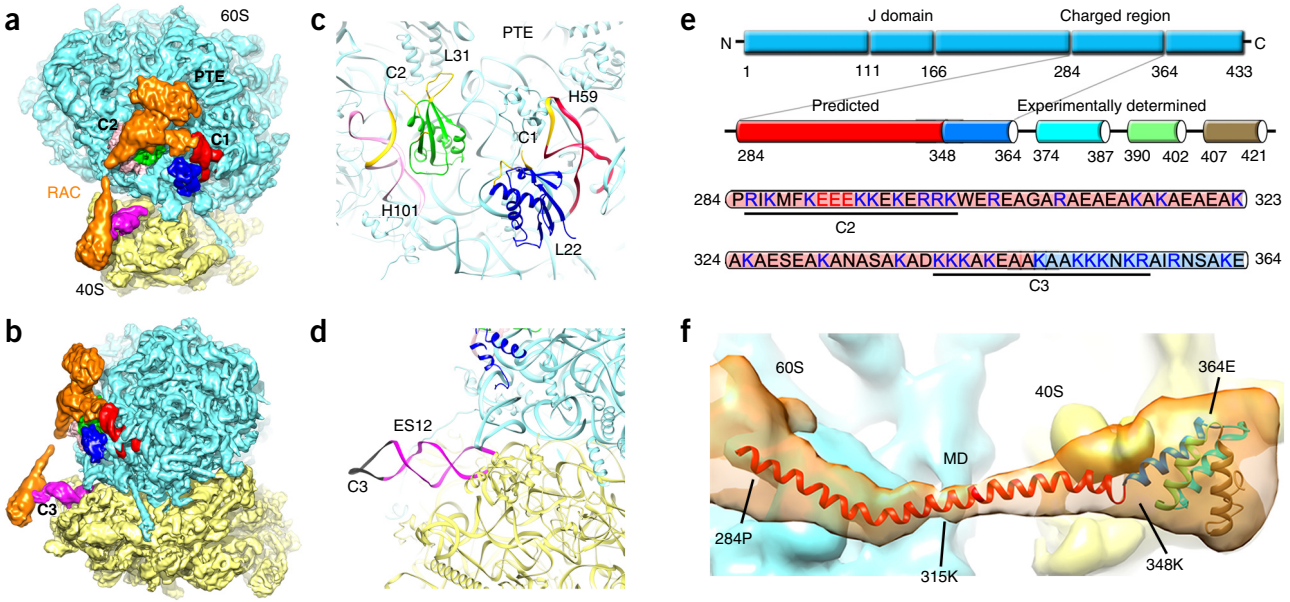

Figure 1 Structural characterization of the ribosome-Zuotin interactions. (**a**,**b**) Cryo-EM density map of the 80S–RAC complex in the nonrotated state, shown in two views. The 60S (cyan), 40S (yellow) and RAC (orange) are separately colored, with three ribosome-Zuotin contacts (C1–C3) indicated. The 4.9-Å density map was filtered to 6 Å to avoid possible overinterpretation. The segmented map of RAC is presented in a lower contour level, owing to substoichiometric binding of factors. (**c**,**d**) Two close-up views of the three ribosome-Zuotin contacts. The ribosomal-component residues in direct contact with Zuotin are highlighted in bright yellow in **c** and in gray in **d**. (**e**) Sequence and secondary-structural analysis of the charged region of Zuotin. The charged region contains a predicted long α-helix (284–364). The atomic structure of residues 348–433 was previously determined (PDB 2LWX)[21]. Positively and negatively charged segments of Zuotin (C2 and C3) involved in interaction with the ribosome are underlined in the sequence (positively charged in blue and negatively charged in red). (**f**) The partial atomic model of Zuotin (284–433), colored as in **e** and superimposed with the segmented density map of Zuotin (from the data set RAC6).

Another inherently flexible component of the 25S rRNA, ES27, also appears to interact with the Zuotin NTD (**Supplementary Fig. 2**).

Structural characterization of the ribosome-RAC contacts

To further improve the structure, we subjected particles to three-dimensional (3D) classification. According to the conformational states of the 80S ribosome, we combined particles from different experimental batches with relatively higher factor occupancy and subjected them to further 3D classification and refinement (Online Methods), which improved the overall resolution of the 80S–RAC complex up to 4.9 Å (**Supplementary Fig. 3** and **Supplementary Movie 2**). However, in the high-resolution structures, the substoichiometric binding and the flexibility of factors cause fragmentation of factor densities, especially for Ssz, and additional classification based on factor occupancy results in density maps with compromised resolutions (**Supplementary Fig. 3**). Nevertheless, with the aid of the yeast crystal structure of the 80S ribosome[24], we could unambiguously identify three independent contact sites for Zuotin from the 4.9-Å map, which involve five distinct ribosomal components (**Fig. 1a–d**). In agreement with previous structural work[23], one 60S contact involves H59 and L22 (**Fig. 1c**). The other 60S contact involves H101 and L31 (**Fig. 1c**), concordantly with the reported cross-linking of Zuotin to L31 (ref. 25). On the 40S side, ES12 is the only component interacting with Zuotin (**Fig. 1d**).

Unfortunately, Zuotin and RAC are intrinsically flexible in solution[23], and atomic structures are available for only the Zuotin CTD[21,23]. Zuotin contains a highly charged region (residues 284 to 364) essential for the ribosome interaction[8]. Secondary-structure prediction reports an extremely high tendency for this region to form a single long helix (**Fig. 1e**) (referred to as the middle domain, MD). To depict details of possible atomic interaction, we modeled the helical structure of the MD *de novo*. We docked the partial atomic model (residues 284–433) together with the atomic model of the Zuotin CTD[21] in the density map and optimized the CTD-ES12 interaction by flexible fitting. Notably, the model agrees well with the corresponding rod-like density mass in both length and shape (**Fig. 1f**). This semiquantitative analysis also clearly reveals the electrostatic nature of the interactions between Zuotin MD and the ribosome, with the two ribosomal-contact sites on Zuotin MD enriched in charged residues, particularly lysines and arginines (C2 and C3, **Fig. 1e**).

RAC stabilizes the 80S ribosome in nonrotated, classical conformation

Intriguingly, RAC binds to the 80S ribosomes in different conformational states characterized by the ratchet-like rotation of the 40S subunit relative to the 60S subunit. The ratchet-like motion[26] is an evolutionarily conserved structural feature of all the ribosomes, and it reflects the dynamic cycle of tRNA translocation and peptide elongation[27]. One of the predominant features of the ratchet-like motion is the global rotation of the body domain of the 40S subunit relative to the 60S subunit around the axis at helix (h) 27 of the 18S rRNA[28], roughly perpendicularly to the plane of the subunit interface. Comparison of RAC in two extreme states (nonrotated and fully rotated) reveals a structural remodeling at both the NTD and CTD of Zuotin (**Fig. 2a–d**). In particular, the Zuotin CTD moves together with ES12 on a scale of 20 Å upon a full ratchet-like motion. ES12 is the eukaryotic-specific expansion of h44 of the 18S rRNA, the helix that extends all the way from the periphery to the decoding center (DC). Naturally, the observation of the subunit bridging by RAC through a single continuous α-helix (MD) suggests that RAC might affect the conformational dynamics of the ribosome and thereby functionally link cotranslational folding with the elongation cycle.

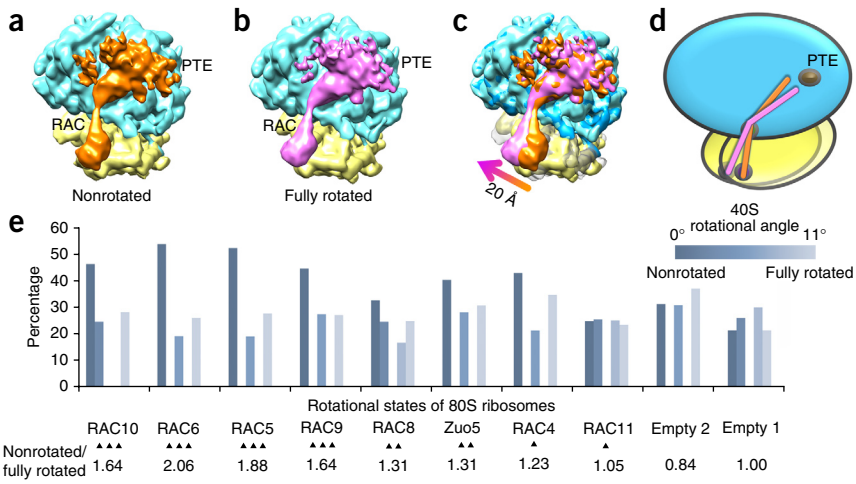

Figure 2 RAC stabilizes the 80S ribosome in a nonrotated conformation. (**a**,**b**) Cryo-EM density maps of nonrotated (**a**) and fully rotated (**b**) ribosomes bound with RAC. The two representative maps were selected from a large number of structures from 3D classification (RAC10 in **Supplementary Table 1**). (**c**) Superposition of the two density maps, with the nonrotated ribosome shown in transparent surface representation. The two maps were aligned with the 60S subunit as a reference. The CTD of Zuotin could move up to 20 Å (arrow) upon a full ratchet-like motion. (**d**) A cartoon model showing the conformational changes of Zuotin. Zuotin appears to rotate around its 60S contacts upon motion of the 80S ribosome. (**e**) Conformational population analysis of the 80S ribosomes, showing RAC-dependent changes in the conformational dynamics of the ribosome. Distributions of particles from ten independent experimental data sets (with more than 90,000 particles; **Supplementary Table 1**) in different conformational states are plotted, according to 3D-classification results. Particles were grouped into five classes on the basis of the extent of 40S body-domain rotation, as indicated by the scale bar (0–11°). Empty 1 and 2 are two independent structural analyses of the 80S ribosome without addition of Zuotin or RAC. Estimated relative factor occupancies in factor-containing reconstructions are indicated by black triangles.

In support of this view, according to our 3D classification of multiple data sets, binding of RAC changes the distribution of equilibrating rotational states of the ribosome, with far more ribosomes in the nonrotated state than in the fully rotated state in the samples with higher occupancy of RAC (RAC10, RAC6, RAC5 and RAC9, **Fig. 2e**). This indicates that the binding of Zuotin poses a constraint for ratchet-like motion and consequently stabilizes the 80S ribosome in a nonrotated state.

The integrity of Zuotin MD is essential for RAC function *in vivo*

Through structural analysis, we found that the Zuotin MD itself constitutes two major ribosome-binding sites (C2 and C3) located exactly at the two ends of the helix: one for the 60S subunit and the other for the 40S subunit (**Supplementary Fig. 4a**). Thus, the MD could, in principle, serve as a perfect signal transmitter between the peptide tunnel exit (PTE) and ES12. To test this idea, we created multiple Zuotin mutants and transfected them into Δ*zuo* (official symbol *zuo1*) or Δ316–433 (C-terminal deletion starting from the middle of Zuotin MD) strains (**Fig. 3**). As expected, the Δ316–433 strain, with a disruption of the MD, had a similar slow-growth phenotype, although to a lesser extent than the Δ*zuo* strain, and a separate construct of the Zuotin C-terminal half (316–433) had no effect in compensating the growth defect of the Δ316–433 cells (**Fig. 3c**). In contrast, a previously reported different C-terminal-deletion strain of Zuotin (Δ364–433), which still possesses a complete MD, had no growth defect in all tested conditions[8]. These data indicate that the physical integrity of Zuotin MD is essential for the full function of RAC. Through sequence analysis of Zuotin MD from multiple species, we found that the length of Zuotin MD appears to have coevolved with that of ES12, with shorter versions of the MDs coinciding with shorter stems of ES12 (**Supplementary Fig. 4**). Following this clue, we demonstrated that progressive lengthening (add4–add8) or shortening (del4–del8) of the length of the MD impaired RAC function *in vivo* exactly as expected (**Fig. 3e**,**f**). To further test the model, we introduced glycine-substituted mutations in the middle of the MD. Consistently with the above results, substantial loss of rigidity in the MD (gly6–gly8) again failed to recover the function of RAC (**Fig. 3g**). Therefore, the continuity, optimal length and rigidity of the Zuotin MD are all required for the *in vivo* function of RAC.

DISCUSSION

The ribosome is a central hub for quality control of newly synthesized proteins[13,29,30]. Regulation of translating ribosomes by elongation pausing or slowdown, often seen to be mediated by structured mRNAs and regulatory polypeptides, appears to be a general

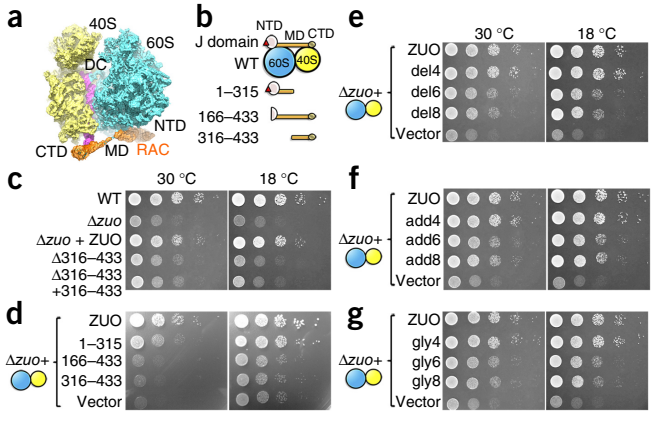

Figure 3 Integrity of the Zuotin MD is essential for RAC function *in vivo*. (**a**) Cryo-EM structure of the 80S–RAC complex (nonrotated state) in conventional front view, showing Zuotin cross-linking of the 60S and 40S subunits through the MD. h44 of the 18S rRNA is colored magenta. (**b**) Schematic cartoons showing the design of plasmids encoding Zuotin mutants. (**c**–**g**) Spot assays showing impaired RAC function *in vivo* in response to changes in the continuity, length or rigidity of the Zuotin MD. Cell-growth tests of the indicated Δ*zuo*, Δ316–433 or wild-type (WT) strains transformed with the indicated YCplac111 vectors (under the endogenous *ZUO1* promoter) encoding full-length Zuotin (ZUO) or residues 316–433 of Zuotin (**c**); full-length or truncated Zuotin as shown in **b** (ZUO, 1–315, 166–433 and 316–433) (**d**); progressive deletions of residues 316–319, 316–321 and 316–323 in Zuotin MD (del4, del6 and del8, respectively) (**e**); progressive insertions of sequences AKAE, AKAEAE and AKAEAEAK before residue A316 in Zuotin MD (add4, add6 and add8, respectively) (**f**); or encoding glycine substitutions of sequences 316–319, 316–321 and 316–323 in Zuotin MD (gly4, gly6 and gly8, respectively) (**g**).

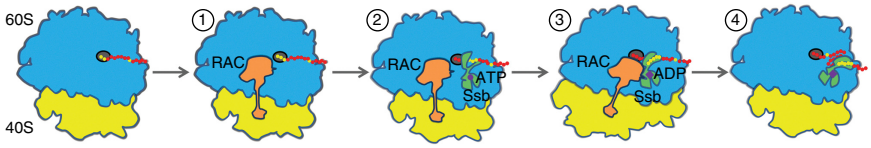

Figure 4 Proposed model of RAC action on a translating ribosome. The emerging aggregation-prone peptide chain signals the ribosome to recruit RAC; RAC binding poses a constraint for intersubunit rotation and therefore reduces elongation rate (1). Ssb binds to aggregation-prone sequences in the ATP-bound state with help of RAC (2). Conformational changes of the Zuotin NTD due to the ratchet-like motion of the 80S ribosome probably reorient Zuotin's J domain to stimulate the ATPase activity of Ssb, thus resulting in high-affinity binding of Ssb–ADP with substrates (3). Ssb in the ADP-bound state protects aggregation-prone sequences until productive folding can occur (4).

scheme adopted by other cellular regulatory processes in translation control[31]. In the present study, we reveal that Zuotin cross-links two ribosomal subunits through a single long α-helix, and binding of RAC changes the conformational dynamics of the ribosome by stabilizing it in a nonrotated state. We further show that any changes in the continuity, length or rigidity of the Zuotin MD impair RAC function *in vivo*. These data suggest that RAC might have a direct role in cotranslational regulation, by modulating the elongation speed of translating ribosomes. Notably, this is in analogy to the action of signal peptide–recognition particle on translating ribosomes (**Supplementary Fig. 5**). The signal peptide–recognition particle also bridges the two subunits and causes translation pausing upon recognition of signal peptide at the PTE[32].

Consistently with this view, RAC–Ssb was shown to be important for translational fidelity[16,17] and polylysine-induced translational repression[15] in yeast as well as for elongation pausing in mammalian cells upon heat shock or proteotoxic stress[18,33]. Notably, a very recent systematic investigation of the RAC–Ssb substrates revealed that these polypeptides have a high aggregation propensity and a low translation rate[14]. These results together with our data support an attractive hypothesis in which elongation of nascent peptides at the heart of the ribosome is synchronized with cotranslational folding at the PTE, and RAC–Ssb is the central player in conveying two-way messages between two functional centers (PTE and DC) of translating ribosomes (**Fig. 4**). On the one hand, RAC could sense folding needs at the PTE and, by binding to the ribosome, constrain the intersubunit motion and cause elongation slowdown or pausing; on the other hand, the ratchet-like motion of the ribosome, through the MD, could induce the structural remodeling of the Zuotin NTD that might tune the binding and function of Ssb[14] .

In summary, we present a structural model for the action of RAC on the eukaryotic ribosome (**Fig. 4**), based on the characterization of the interaction between the empty 80S ribosome and RAC. These data not only contribute to the mechanistic understanding of RAC–Ssb–facilitated cotranslational folding on the ribosome but also provide a structural framework that opens a new avenue for studying the regulatory roles of ribosome-associated chaperones in translation control. Nevertheless, further detailed structural and functional depiction of RAC together with Ssb on the 80S ribosome would require a more functionally relevant translating ribosome that bears native substrates of RAC–Ssb.

METHODS

Methods and any associated references are available in the online version of the paper.

Accession codes. The density maps of the 80S–RAC complex at resolutions of 10.2 Å (total reconstruction from data set RAC6), 7.2 Å and 5.2 Å (nonrotated state) have been deposited in the Electron Microscopy Data Bank under accession codes 6103, 6104 and 6105, respectively.

Note: Any Supplementary Information and Source Data files are available in the online version of the paper.

ACKNOWLEDGMENTS

We thank J. Frank and H. Wang for helpful discussion and critical reading of the manuscript. We acknowledge the China National Center for Protein Sciences (Beijing) and the Explorer 100 cluster system of the Tsinghua National Laboratory for Information Science and Technology for providing computation resources. This work was supported by grants from the National Natural Science Foundation of China (31422016 and 31470722 to N.G.), the Ministry of Science and Technology of China (2010CB912402 and 2013CB910404 to N.G.; 2010CB912401 to J.L.) and the Beijing Higher Education Young Elite Teacher Project (YETP0131 to N.G.).

AUTHOR CONTRIBUTIONS

Y.Z., J.L. and N.G. designed experiments and analyzed data. Y.Z. performed protein preparation, ribosome purification (together with C.M. and S.W.), data collection (together with Y.Y.), image processing (together with N.L.) and spot assays. J.Z., C.C. and L.Y. contributed to yeast-strain and plasmid construction. Y.Z. and N.G. wrote the manuscript; L.Y. commented on the manuscript; and all authors approved the final manuscript.

COMPETING FINANCIAL INTERESTS

The authors declare no competing financial interests.

1. Hartl, F.U. & Hayer-Hartl, M. Converging concepts of protein folding *in vitro* and *in vivo*. *Nat. Struct. Mol. Biol.* **16**, 574–581 (2009).
2. Kramer, G., Boehringer, D., Ban, N. & Bukau, B. The ribosome as a platform for co-translational processing, folding and targeting of newly synthesized proteins. *Nat. Struct. Mol. Biol.* **16**, 589–597 (2009).
3. Preissler, S. & Deuerling, E. Ribosome-associated chaperones as key players in proteostasis. *Trends Biochem. Sci.* **37**, 274–283 (2012).
4. Hundley, H.A., Walter, W., Bairstow, S. & Craig, E.A. Human Mpp11 J protein: ribosome-tethered molecular chaperones are ubiquitous. *Science* **308**, 1032–1034 (2005).
5. Otto, H. *et al.* The chaperones MPP11 and Hsp70L1 form the mammalian ribosome-associated complex. *Proc. Natl. Acad. Sci. USA* **102**, 10064–10069 (2005).
6. Gautschi, M., Mun, A., Ross, S. & Rospert, S. A functional chaperone triad on the yeast ribosome. *Proc. Natl. Acad. Sci. USA* **99**, 4209–4214 (2002).
7. Gautschi, M. *et al.* RAC, a stable ribosome-associated complex in yeast formed by the DnaK-DnaJ homologs Ssz1p and zuotin. *Proc. Natl. Acad. Sci. USA* **98**, 3762–3767 (2001).
8. Yan, W. *et al.* Zuotin, a ribosome-associated DnaJ molecular chaperone. *EMBO J.* **17**, 4809–4817 (1998).
9. Nelson, R.J., Ziegelhoffer, T., Nicolet, C., Werner-Washburne, M. & Craig, E.A. The translation machinery and 70 kd heat shock protein cooperate in protein synthesis. *Cell* **71**, 97–105 (1992).
10. Hundley, H. *et al.* The *in vivo* function of the ribosome-associated Hsp70, Ssz1, does not require its putative peptide-binding domain. *Proc. Natl. Acad. Sci. USA* **99**, 4203–4208 (2002).
11. Huang, P., Gautschi, M., Walter, W., Rospert, S. & Craig, E.A. The Hsp70 Ssz1 modulates the function of the ribosome-associated J-protein Zuo1. *Nat. Struct. Mol. Biol.* **12**, 497–504 (2005).
12. Kampinga, H.H. & Craig, E.A. The HSP70 chaperone machinery: J proteins as drivers of functional specificity. *Nat. Rev. Mol. Cell Biol.* **11**, 579–592 (2010).
13. Pechmann, S., Willmund, F. & Frydman, J. The ribosome as a hub for protein quality control. *Mol. Cell* **49**, 411–421 (2013).
14. Willmund, F. *et al.* The cotranslational function of ribosome-associated Hsp70 in eukaryotic protein homeostasis. *Cell* **152**, 196–209 (2013).
15. Chiabudini, M., Conz, C., Reckmann, F. & Rospert, S. Ribosome-associated complex and Ssb are required for translational repression induced by polylysine segments within nascent chains. *Mol. Cell. Biol.* **32**, 4769–4779 (2012).

16. Rakwalska, M. & Rospert, S. The ribosome-bound chaperones RAC and Ssb1/2p are required for accurate translation in *Saccharomyces cerevisiae*. *Mol. Cell. Biol.* **24**, 9186–9197 (2004).
17. Muldoon-Jacobs, K.L. & Dinman, J.D. Specific effects of ribosome-tethered molecular chaperones on programmed –1 ribosomal frameshifting. *Eukaryot. Cell* **5**, 762–770 (2006).
18. Liu, B., Han, Y. & Qian, S.B. Cotranslational response to proteotoxic stress by elongation pausing of ribosomes. *Mol. Cell* **49**, 453–463 (2013).
19. Koplin, A. *et al.* A dual function for chaperones SSB-RAC and the NAC nascent polypeptide-associated complex on ribosomes. *J. Cell Biol.* **189**, 57–68 (2010).
20. Albanèse, V., Reissmann, S. & Frydman, J. A ribosome-anchored chaperone network that facilitates eukaryotic ribosome biogenesis. *J. Cell Biol.* **189**, 69–81 (2010).
21. Ducett, J.K. *et al.* Unfolding of the C-terminal domain of the J-protein Zuo1 releases autoinhibition and activates Pdr1-dependent transcription. *J. Mol. Biol.* **425**, 19–31 (2013).
22. Prunuske, A.J., Waltner, J.K., Kuhn, P., Gu, B. & Craig, E.A. Role for the molecular chaperones Zuo1 and Ssz1 in quorum sensing via activation of the transcription factor Pdr1. *Proc. Natl. Acad. Sci. USA* **109**, 472–477 (2012).
23. Leidig, C. *et al.* Structural characterization of a eukaryotic chaperone—the ribosome-associated complex. *Nat. Struct. Mol. Biol.* **20**, 23–28 (2013).
24. Ben-Shem, A. *et al.* The structure of the eukaryotic ribosome at 3.0 Å resolution. *Science* **334**, 1524–1529 (2011).
25. Peisker, K. *et al.* Ribosome-associated complex binds to ribosomes in close proximity of Rpl31 at the exit of the polypeptide tunnel in yeast. *Mol. Biol. Cell* **19**, 5279–5288 (2008).
26. Frank, J. & Agrawal, R.K. A ratchet-like inter-subunit reorganization of the ribosome during translocation. *Nature* **406**, 318–322 (2000).
27. Frank, J., Gao, H., Sengupta, J., Gao, N. & Taylor, D.J. The process of mRNA-tRNA translocation. *Proc. Natl. Acad. Sci. USA* **104**, 19671–19678 (2007).
28. Spahn, C.M. *et al.* Domain movements of elongation factor eEF2 and the eukaryotic 80S ribosome facilitate tRNA translocation. *EMBO J.* **23**, 1008–1019 (2004).
29. Sherman, M.Y. & Qian, S.B. Less is more: improving proteostasis by translation slow down. *Trends Biochem. Sci.* **38**, 585–591 (2013).
30. Shoemaker, C.J. & Green, R. Translation drives mRNA quality control. *Nat. Struct. Mol. Biol.* **19**, 594–601 (2012).
31. Ingolia, N.T. Ribosome profiling: new views of translation, from single codons to genome scale. *Nat. Rev. Genet.* **15**, 205–213 (2014).
32. Halic, M. *et al.* Structure of the signal recognition particle interacting with the elongation-arrested ribosome. *Nature* **427**, 808–814 (2004).
33. Shalgi, R. *et al.* Widespread regulation of translation by elongation pausing in heat shock. *Mol. Cell* **49**, 439–452 (2013).

ONLINE METHODS

Protein purification. The *S. cerevisiae* (S288C) genes (*ZUO1* and *SSZ1*) encoding full-length Zuotin and Ssz were cloned into the coexpression vector pETduet1, to create a pETduet1-ZUO1-SSZ1 plasmid. The plasmid was transformed into *Escherichia coli* BL21 cells for overexpression. Cells were induced at 28 °C with 1 mM IPTG for 8 h, harvested, resuspended in buffer A (20 mM HEPES, 120 mM KOA_C, 10 mM $Mg(OA_C)_2$, 1 mM PMSF, and 10 mM imidazole, pH 7.4) and subjected to ultrasonic lysis. The cell lysates were then clarified by centrifugation at 15,000*g* for 30 min. Supernatants were loaded onto a Ni-NTA column (GE Healthcare) and eluted with buffer B (20 mM HEPES, 120 mM KOA_C, 10 mM $Mg(OA_C)_2$, 1 mM PMSF, and 250 mM imidazole, pH 7.4). Eluates were further purified with a Resource Q column (1 ml, GE Healthcare). The RAC-containing fractions were pooled, concentrated and loaded onto a preequilibrated Superdex 200 column (10/300 GL, GE Healthcare) with buffer C (20 mM HEPES, 120 mM KOA_C, 10 mM $Mg(OA_C)_2$, and 1 mM PMSF, pH 7.4). For separate Zuotin preparation, the gene encoding full-length Zuotin was cloned into pET28a plasmid. *E. coli* BL21 cells containing pET-ZUO1 were induced at 25 °C for 10 h, and purification was done similarly.

Ribosome purification. Cells of the *S. cerevisiae* S288C strain were grown in 3 l of YPD medium to an OD_{600} of 1.0, harvested and washed twice with 200 ml ice-cold lysis buffer (30 mM Tris-acetate, 100 mM NH_4Cl, 12 mM $MgCl_2$, and 2 mM DTT, pH 7.0). Resuspended cells were disrupted by a high-pressure homogenizer. Cell lysates were clarified by centrifugation at 13,000 r.p.m. for 30 min at 4 °C in a JA 25.50 motor (Beckman Coulter) and subjected to sucrose cushion–based centrifugation (1 M sucrose, 50 mM Tris-acetate, 500 mM NH_4Cl, 12 mM $MgCl_2$, and 2 mM DTT, pH 7.4) at 30,000 r.p.m. for 20 h in a Ti70 rotor (Beckman Coulter) at 4 °C. The pellets were resuspended and layered onto a linear 10–50% sucrose density gradient (same buffer) and subjected to centrifugation at 28,000 r.p.m. for 7 h in a SW28 rotor (Beckman Coulter) at 4 °C. The gradients were then monitored by absorption at 260 nm and fractionated in a gradient collector (Teledyne Isco). The pooled 80S ribosomes were concentrated with Amicon Ultra centrifugal filter units (Millipore) at 3,000*g*, with buffer changed to buffer C for storage.

Cryo-sample preparation and data collection. The 80S ribosomes were incubated with RAC or Zuotin in a ratio of 1:80 for 20 min at 30 °C. The reaction mixture was centrifuged at 14,000*g* for 5 min to remove possible aggregates. The supernatants were collected and diluted to a final concentration of ~60 nM. 4-µl aliquots of diluted samples were loaded onto 300-mesh glow-discharged Quantifoil 2/2 grids, which were coated with a thin layer of freshly prepared carbon film (~10-nm thickness). Blotting and plunging into liquid ethane were done in an FEI Mark IV Vitrobot operated at 4 °C and 90% humidity. Grids were examined, and images were collected in an FEI Titan Krios at 300 kV with an FEI Eagle 4,000 × 4,000 CCD camera or in an FEI Tecnai F20 at 200 kV with a Gatan UltraScan 4000 CCD camera (**Supplementary Table 1**). All images were collected with the AutoEMation package[34] under low-dose conditions (20 $e^-/Å^2$).

Image processing and analysis. Multiple data sets from different batches of biological experiments were processed similarly (**Supplementary Table 1**). Preprocessing of micrographs (micrograph screening and estimation of contrast transfer function parameters) and particle picking were done with the SPIDER package[35]. Particle images (decimated by a factor of two, pixel size 2.33 Å) were quickly screened manually with a classification-based method[36]. Particles were then subjected to 3D classification (six or more classes in 35 iterations with a final angular sampling of 0.9°) with the RELION package[37], which revealed different conformational states for the 80S ribosome, characterized by the extent of intersubunit rotation (**Supplementary Table 1**). On the basis of 3D-classification results, nondecimated particle images (360 × 360; pixel size, 1.166 Å) from reconstructions with the highest occupancy for RAC (RAC5, RAC9 and RAC10) were combined and subjected to further 3D classification and structural refinement. As a result, 318,404 and 125,245 particles (both from Titan Krios) in nonrotated and fully rotated states, respectively, were used for final reconstruction. Refinements were performed with both SPIDER and RELION packages, and no significant differences were found. The final density maps were further processed (*B*-factor sharpening) with the postprocessing program in RELION. The resolution was determined with the gold-standard Fourier shell correlation (FSC) 0.143 criterion, resulting in 4.9 Å and 5.9 Å for nonrotated and fully rotated states, respectively. However, in the high-resolution structures, the substoichiometric binding and the flexibility of factors resulted in fragmentation of factor densities, especially at the location of the Ssz CTD (comparison of **Fig. 1a** with **Supplementary Fig. 1d**). To further explore the classification for the nonrotated state, the combined 318,404 particles were subjected to another round of 3D classification with RELION (**Supplementary Fig. 3**). Particles in slightly rotated classes were removed in this step, and only particles in a defocus range of –1.5 µm to –3.5 µm were kept. Subsequently, 167,534 particles for the nonrotated state were kept for further refinement, thus resulting in a 5.2-Å density map with improved resolution for the head domain of the 40S subunit but no significant differences for the 60S subunit. To further improve the occupancy of Zuotin on the 80S ribosome, a third round of multiple-reference 3D classification based on RELION was applied. The orientation and translation parameters of particles from the previous round of high-resolution refinement were relatively fixed, and the classification was restricted to a relatively small local search, with a rotational search restriction of 5°. Two reference maps were supplied: the nonrotated map from the data set RAC6 (higher Zuotin occupancy) and the nonrotated map from the data set Empty 2 (no Zuotin density). As a result, 167,534 particles were classified in two groups, and 75,055 particles, according to higher occupancy of Zuotin, were kept. The same procedures were repeated once more with the 75,055 particles as the input data set. Finally, 24,619 particles with stronger Zuotin density were kept and refined to a 7.2-Å map (**Supplementary Fig. 3** and **Supplementary Movie 2**). Local resolution maps of the 4.9-Å, 5.2-Å and 7.2-Å maps, obtained with ResMap[38], and FSC curves are presented in **Supplementary Figure 6**.

The full-length Zuotin secondary-structural prediction was performed with the PSIPRED web server[39] (http://bioinf.cs.ucl.ac.uk/psipred/). 3D structural modeling of full-length Ssz1 and Zuotin MD fragment (284–348) were performed with I-TASSER[40], with the crystal structure of a bovine Hsc70 chaperone (PDB 1YUW)[41] and the α-helical structure of keratin (PDB 3TNU)[42] as templates. The I-TASSER–derived Zuotin MD (284–348) model was then combined with the NMR-determined Zuotin CTD structure (348–433) (PDB 2LWX)[21]. The partial atomic model of Zuo1 (284–433) was manually docked in the cryo-EM density maps of the 80S–RAC complex, and interactions of the Zuotin CTD with ES12 were optimized with a flexible-fitting approach (molecular dynamics flexible fitting)[43] with the NAMD package[44]. Chimera[45] and PyMOL (http://www.pymol.org/) were used for structural analysis and figure preparation.

Yeast strains and plasmids. The deletion strains (BY4741) lacking ZUO1 (Δ*zuo*) or $ZUO1_{316–433}$ (Δ316–433) were obtained by replacement of *ZUO1* or $ZUO1_{316–433}$ with *zuo1*::*hphNT1* and $zuo1_{316–433}$::*hphNT1* deletion cassettes. The ZUO1 upstream (+435 bp) PstI/NcoI (NEB) fragment, full-length ZUO1 NcoI/NotI coding sequence and ZUO1 downstream (–476 bp) NotI/BamHI fragment were PCR-cloned from the *S. cerevisiae* genome (S288C), ligated and inserted into the PstI/BamHI double-digested YCplac111 plasmid (single copy number), thus creating a vector version of ZUO1 under its endogenous promoter (YCplac111-ZUO1). A series of Zuotin MD deletions (del4, del6, and del8) were constructed by replacement of ZUO1 in the YCplac111-ZUO1 vector with PCR-cloned ZUO1Δ316–319, ZUO1Δ316–321, and ZUO1Δ316–323 PstI/BamHI fragments, respectively. Insertion mutations of Zuotin MD (add4, add6, and add8) were similarly constructed by insertion of AKAE, AKAEAE, and AKAEAEAK, respectively, before residue 316A of ZUO1 in the YCplac111-ZUO1 vector. Substitution mutations of Zuotin MD (gly4, gly6, and gly8) were also constructed by replacement of corresponding sequences of ZUO1 (316–319, 316–321, and 316–323, respectively) in the YCplac111-ZUO1 vector with glycines. Three additional ZUO1-truncation mutants, YCplac111-$ZUO1_{1–315}$, YCplac111-$ZUO1_{316–433}$ and YCplac111-$ZUO1_{166–433}$, were similarly obtained. YCplac111 plasmids carrying different ZUO1 mutants were transformed into Δ*zuo* or Δ316–433 strains. The logarithmic-phase cells were spotted as a ten-fold dilution series on YPD plates and grown at 18 °C or 30 °C, for ~48 h or 24 h, respectively.

34. Lei, J. & Frank, J. Automated acquisition of cryo-electron micrographs for single particle reconstruction on an FEI Tecnai electron microscope. *J. Struct. Biol.* **150**, 69–80 (2005).
35. Shaikh, T.R. *et al.* SPIDER image processing for single-particle reconstruction of biological macromolecules from electron micrographs. *Nat. Protoc.* **3**, 1941–1974 (2008).

36. Shaikh, T.R., Trujillo, R., LeBarron, J.S., Baxter, W.T. & Frank, J. Particle-verification for single-particle, reference-based reconstruction using multivariate data analysis and classification. *J. Struct. Biol.* **164**, 41–48 (2008).
37. Scheres, S.H. A Bayesian view on cryo-EM structure determination. *J. Mol. Biol.* **415**, 406–418 (2012).
38. Kucukelbir, A., Sigworth, F.J. & Tagare, H.D. Quantifying the local resolution of cryo-EM density maps. *Nat. Methods* **11**, 63–65 (2014).
39. Buchan, D.W., Minneci, F., Nugent, T.C., Bryson, K. & Jones, D.T. Scalable web services for the PSIPRED Protein Analysis Workbench. *Nucleic Acids Res.* **41**, W349–W357 (2013).
40. Roy, A., Kucukural, A. & Zhang, Y. I-TASSER: a unified platform for automated protein structure and function prediction. *Nat. Protoc.* **5**, 725–738 (2010).
41. Jiang, J., Prasad, K., Lafer, E.M. & Sousa, R. Structural basis of interdomain communication in the Hsc70 chaperone. *Mol. Cell* **20**, 513–524 (2005).
42. Lee, C.H., Kim, M.S., Chung, B.M., Leahy, D.J. & Coulombe, P.A. Structural basis for heteromeric assembly and perinuclear organization of keratin filaments. *Nat. Struct. Mol. Biol.* **19**, 707–715 (2012).
43. Trabuco, L.G., Villa, E., Mitra, K., Frank, J. & Schulten, K. Flexible fitting of atomic structures into electron microscopy maps using molecular dynamics. *Structure* **16**, 673–683 (2008).
44. Phillips, J.C. *et al.* Scalable molecular dynamics with NAMD. *J. Comput. Chem.* **26**, 1781–1802 (2005).
45. Pettersen, E.F. *et al.* UCSF Chimera: a visualization system for exploratory research and analysis. *J. Comput. Chem.* **25**, 1605–1612 (2004).

doi:10.1038/nsmb.2908